Research Article

Facile Synthesis of Hybrid-Polyoxometalates Nanocomposite for Degradation of Cationic and Anionic Dyes in Water Treatment

Wei Wei Leow and Alvin Duke
Faculty of Chemical Engineering & Technology, Universiti Malaysia Perlis (UniMAP), Perlis, Malaysia

Siti Kartini Enche Ab Rahim*, Qi Hwa Ng, Peng Yong Hoo and Amira Mohd Nasib
Faculty of Chemical Engineering & Technology, Universiti Malaysia Perlis (UniMAP), Perlis, Malaysia
Centre of Excellence for Frontier Materials Research (CFMR), Universiti Malaysia Perlis (UniMAP), Perlis, Malaysia

Muhamad Qauyum Zawawi Ahamad Suffin
Faculty of Mechanical Engineering & Technology, Universiti Malaysia Perlis, Kampus Utama Pauh Putra, Arau, Perlis, Malaysia

Norazharuddin Shah Abdullah
School of Materials and Mineral Resources Engineering, Universiti Sains Malaysia, Engineering Campus, Nibong Tebal, Penang, Malaysia

* Corresponding author. E-mail: sitikartini@unimap.edu.my DOI: 10.14416/j.asep.2024.07.014
Received: 16 April 2024; Revised: 30 May 2024; Accepted: 14 June 2024; Published online: 26 July 2024

Abstract
Photocatalysis emerges as a promising method for treating organic dye contaminated wastewater. This process involves the use of photocatalysts through light activation, typically semiconductors such as titanium dioxide (TiO_2) or polyoxometalates (POM) to generate reactive species capable of degrading organic pollutants. Several factors influence the photodegradation of ionic and cationic dyes including chemical properties, reaction mechanism and degradation efficiency. This work evaluated photodegradation performance of methyl orange (MO) and malachite green (MG) dyes using hybrid-polyoxometalate (HPOM) photocatalyst. Fourier Transform Infrared Spectroscopy (FTIR) identified the characteristic band at 3463.66 cm^{-1} (O-H) and 997.74 cm^{-1} (W-O). Scanning Electron Microscopy (SEM) revealed the presence of rod-like and granular structures in HPOM, representing silver acetate and sodium tungstate. X-ray diffraction (XRD) confirmed characteristic peak of Keggin structure, revealing high crystallinity of HPOM. UV-assisted photodegradation was evaluated on different parameters (initial dye concentration, photocatalyst dosage and pH), highlighting HPOM's better affinity for degrading cationic dye. The optimum photodegradation conditions for MG and MO dyes were 20 ppm dye concentration, 100 mg photocatalyst dosage, and pH 7 and 8, respectively. The kinetic data was fitted with the Langmuir Hinshelwood kinetic model, indicating pseudo-first-order kinetics. HPOM exhibited a higher rate constant, k for MG (k = 0.0068 min^{-1}) than MO (k = 0.0029 min^{-1}).

Keywords: Dyes, Kinetics, Photocatalysis, Photodegradation, Polyoxometalate

1 Introduction

Dyes serve as a pervasive coloring agent across various industries such as food, pharmaceuticals, textiles, cosmetics, and other crucial industries. The ease of the synthesis process and fade resistance render the dyes favorable, and widespread adoption in the industries. However, the rapid development in industrialization

has led to a substantial increase in dye usage, generating a substantial amount of wastewater over the decades [1]. Synthetic dyes foster a colorful world, accompanying the water pollution problem, as dyes are reported as a contaminants commonly found in wastewater streams. Dyes can be classified into natural dyes and synthetic dyes. Natural dyes, derived from naturally occurring sources like lutein extracted from plant, produce a high amount of wastewater during squeezing process [2]. Due to the high cost and limited colorfastness properties of natural dyes, synthetic dyes have become the preferred choice across various industries [3]. Driven by the rising demand for manufactured and high-quality products, the manufacturing industries require large amounts of dyes to enhance the product's appearance, although only a minimal portion of dye molecules bind to the fabric [4]. A large quantity of water is required to wash the fabric and excessive chemical compounds like dyes, acids and alkaline during dyeing [5], [6]. Unfortunately, the improper wastewater treatment process causes the dye effluent to persist in waterbodies and remain untreated before releasing the wastewater into the environment [4]. The massive amount of aqueous dye effluent combination discharged without proper treatment can pose an environmental challenge. The discharged wastewater comprises various dyes in different compositions especially anionic and cationic dyes [6]. Methyl orange (MO) and malachite green (MG) are synthetic dyes commonly used in the textile industry due to their cost-effectiveness and high availability, which exemplify this environmental issue. MO is an anionic azo dye with a negative charge, and MG is a cationic dye that belongs to the triphenylmethane dye category [7]. Both dyes are mutagenic and carcinogenic as arise from their structures that consist of aromatic rings structure, posing significant health risks [8], [9]. A small amount of these dyes can cause severe health issues, impacting human development and health. Therefore, water pollution issue has been highlighted and need to take action to find an approach to treatment.

There are various pollutant removal methods such as adsorption [7], biological treatment [2], membrane separation [10], etc. However, these methods exhibit limitations, such as high cost, long time consumption and secondary wastes [11]. Photocatalysis is an advanced oxidation process that utilizes solar energy to effectively degrade pollutants such as dyes [12]. This process can break down organic compounds completely by generating highly reactive hydroxyl radicals, turning the compounds into water, carbon dioxide and other inorganic ions [13]. This process is assisted with the aid of photocatalyst and irradiation. The presence of semiconductor photocatalyst, such as titanium oxide (TiO_2), zinc oxide (ZnO) and zinc sulfide (ZnS) facilitates the degradation process. TiO_2 and ZnO_2 are the most notable metal oxide semiconductor photocatalysts that are widely used in industries due to their low cost, non-toxicity and chemical stability [14]. The photocatalysis process for dye wastewater treatment has been focused and the use of photocatalyst has been reported [15], [16]. Meso-TiO_2 photocatalyst synthesized by bi-template assisted sol-gel method showed maximum degradation of 62.3554% on MO [15]. ZnO nanoparticles showed 95.41% of photocatalytic degradation in Rhodamine B dye revealing high photocatalytic efficiency [16]. However, the wide band gap of metal oxide semiconductors, which only allow it to generate radicals under UV light exposure and the fast recombination of electrons and holes also decrease the photocatalytic degradation performance [15], [17].

Polyoxometalates (POMs), the transition metals substituted clusters exhibiting unique properties, such as redox [18], are reportedly combined with organic ligands and transition metal ions to yield the heterogeneous, hybrid-polyoxometalate (HPOM) [19]. HPOM can be categorized depending on the integrated counterpart in the structure and exhibit either ionic or covalent interaction. The encapsulation of catalytically active POMs in the metal-organic framework is known as one of the ionic interactions of POMs with organic counterparts. For the covalent interaction with organic counterparts, the HPOM with enhanced stability was formed due to the covalent bond [20].

Four common structures of POMs were studied due to their versatility: Lindqvist, Anderson-Evans, Keggin, and Wells-Dawson [21]. Keggin-structured polyoxometalate is one of the most reviewed and reported in photocatalysis due to its exceptional stability and catalytic properties under reaction conditions [11], [22]. The Keggin structure is characterized by a central heteroatom and four trimetallic groups, forming high porosity due to the crystallite pores [20], [23]. The strong covalent dative bonds between oxygen atoms and metal ions were attributed to their high chemical and mechanical resistance properties. Keggin structure polyoxometalate is also efficient in electron accepting and storing due to the vacant d orbitals in Keggin structure that facilitate the electron transfer reactions [24], [25]. HPOM shows higher efficiency in photocatalytic degradation as it improves the generation of reactive OH radicals and complete organic compound conversion [26], [27].

The discharged industrial wastewater consists of mixed dye effluents and other pollutants [28]. The separation of chemicals from the water is a challenge encountered. Photocatalytic degradation has been one of the promising strategies in pollutant removal [29]. Therefore, in this study, a heterogenous Keggin-type hybrid polyoxometalate was synthesized using hydrothermal technique, characterized and used as the photocatalyst in treating different types of dye solutions. The photocatalytic degradation ability in the cationic and the anionic dye of the synthesized photocatalyst was also evaluated and compared with MO and MG in the effect of initial concentration of dye solution, photocatalyst dosage and pH. Moreover, the kinetics of the MO and MG dyes were also investigated to study the degradation performance of photocatalytic systems by determining the degradation rate of the reactions.

2 Materials and Methods

2.1 *Materials*

Sodium tungstate dihydrate ($Na_2WO_4 \cdot 2H_2O$), Silver acetate ($Ag(CH_3CO_2)$) 1H-benzotrialzole and 4,4'-bipyridine were purchased from Merck, Germany. Hydrochloric acid (HCl, 37%) was obtained from J. T. Baker, sodium hydroxide (NaOH) was obtained from HmbG Chemicals, ethanol (CH_3COOH, 99%) was obtained from VWR Chemical, malachite green (MG, 90%) and methyl orange (MO, 85%) from Sigma-Aldrich were of analytical used and without further purification. All chemicals used were reagent grade without further purification.

2.2 *Synthesis HPOM photocatalyst*

Hybrid-polyoxometalates (HPOM) were synthesized in a Teflon-lined hydrothermal synthesis autoclave. Specifically, silver acetate, $Ag(CH_3CO_2)$, 1H-benzotrialzole, 4,4'-bypyridine (weight ratio 3:1:1) and deionized water were dissolved in a beaker and followed by stirring vigorously for 30 min. Sodium tungstate dihydrate, $Na_2WO_4 \cdot 2H_2O$, was added to the solution and stirred vigorously until a cloudy solution formed. The initial pH value of the solution was measured using a pH meter and controlled in the range of pH 2 to 3 using hydrochloric acid (HCl) solution. The solution was hydrothermally heated in a 10 mL Teflon-lined hydrothermal synthesis autoclave reactor for 72 h. After cooling to room temperature, the solution was sent to the refrigerator to be stored at 4 °C for 1 day. The mixture was filtered, extracted, and purified using ethanol and deionized water. The drying process was carried out at 70 °C until dried to obtain a powdered state, yielding HPOM.

2.3 *Characterization*

The structure of HPOM was analyzed using Fourier Transform Infrared Spectroscopy (FTIR, PerkinElmer Spotlight™ Fourier Transform Infrared Spectroscopy 400 Microscopy). To carry out FTIR analysis, potassium bromide (KBr) was used as the carrier for the sample. The photocatalyst was mixed with KBr and transferred into a pellet die to be pressed into a diss. The disc was then transferred and placed in the sample holder for analysis. Besides, the morphology of the synthesized photocatalyst was also examined with Scanning Electron Microscopy (SEM, JEOL JSM 6460LA). The electron microscope with a resolution of 0.126 keV and an acceleration voltage of 20 kV were used to observe the surface morphology of the photocatalyst. The composition of the photocatalyst was also studied using Energy Dispersive X-ray spectroscopy (EDX). The crystal structure of the photocatalyst was determined and obtained by X-ray diffractor (XRD, Bruker D2 PHASER). The powder X-ray diffractometer with copper (Cu) X-ray tube was used and the wavelength was Kα1= 1.5406 Å. The XRD was generated at 10 mA and 30 Kv to find out the compound structure that existed in the synthesized photocatalyst.

2.4 *Photocatalytic study*

The photocatalytic degradation was carried out on MO and MG dye using a photocatalytic batch reactor under ultraviolet (UV) irradiation, as illustrated in Figure 1. The experiments were carried out in the dark to investigate the photocatalytic degradation efficiency and the adsorption of MO and MG to the HPOM. Specific combinations of dye concentration and amount of photocatalyst were introduced into a 1 L reactor (height 31 cm, diameter 8 cm, wall thickness 1 cm). A 220 VAC UV photochemical lamp with its radiation at 254 nm (lamp length 27.94 cm, diameter 0.95 cm) was immersed into the dye solution. The solution was stirred for 180 min using a magnetic stirrer. The sample of suspension was collected for each 10 min over 180 min. The absorbance of samples was measured by UV-vis spectrophotometer (UV-Vis, Shimadzu UV-1800) using absorption wavelength of MO and MG at 464 nm and 617 nm, respectively, to measure the concentration of dye and determine the reaction of photocatalytic degradation.

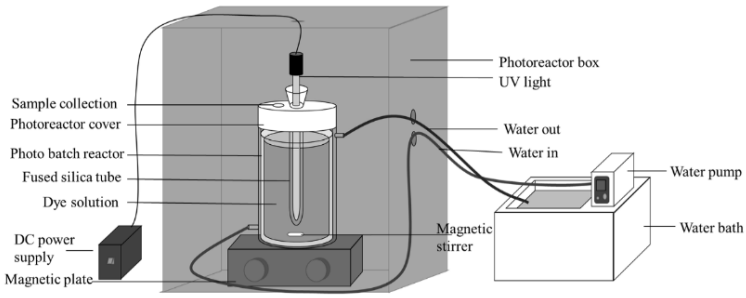

Figure 1: Photocatalytic degradation experiment setup.

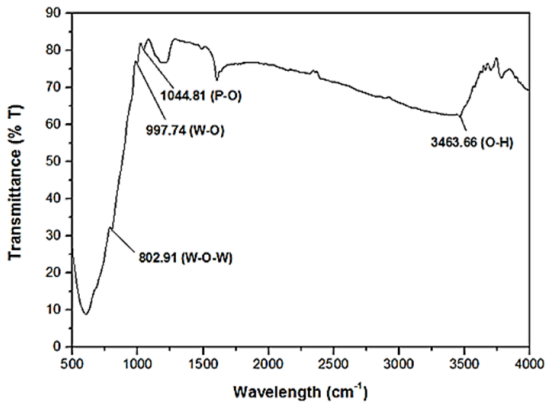

Figure 2: FTIR spectra of the synthesized HPOM.

2.5 *Effect of initial concentration of dye*

The effect of the initial concentration of MO and MG dyes was examined using 20 ppm, 40 ppm, 60 ppm, 80 ppm, and 100 ppm dye concentrations. The temperature remained at room temperature (25 °C) and the pH of the solution remained constant. The 10 mg of HPOM photocatalyst and 1 L of dye solution were introduced into the reactor and stirred for 180 min at room temperature.

2.6 *Effect of HPOM dosage*

The experiments were carried out in different photocatalyst dosages: 20 mg, 40 mg, 60 mg, 80 mg, and 100 mg. The temperature remained at room temperature (25 °C) and the pH remained constant. 20 ppm of dye solution was used for each photocatalyst dosage. At room temperature, 1 L of 20 ppm concentration dye solution was stirred for 180 min.

2.7 *Effect of pH*

The effect of pH value was examined by pH 2, 4, 6, 7, 8, and 10. 10 mg of HPOM was added to 1L of 20 ppm dye solution before being agitated for 180 min at room temperature (25 °C). The pH value was adjusted by adding HCl and NaOH while other parameters remained constant.

3 Results and Discussion

3.1 *Characterization*

3.1.1 Fourier Transform Infrared Spectroscopy (FTIR) Analysis

The functional groups of HPOM photocatalyst were identified by FTIR and analyzed in Figure 2 by observing the apparent peaks of the Keggin cluster at 802.91, 997.74, 1044.81, and 3463.66 cm^{-1}.

The peak at 802.91 cm^{-1} was associated with the W-O-W group, while the peak at 997.74 cm^{-1} corresponds to the W=O group. The peaks of 1044.81 and 3463.66 cm^{-1} were attributed to P-O bonding and the vibration of hydrogen bonding (O-H bond), respectively [26], [30], [31]. The O-H vibration bond was found in the synthesized photocatalyst as the presence of the hydroxyl group on the catalyst's surface was to play a crucial role in enhancing the photocatalytic activity of HPOM. The O-H bond has stronger strength than the van der Waals bond. The interaction of the O-H bond and the photogenerated holes affects the recombination rate of photogenerated electron and hole pairs [32].

3.1.2 Scanning Electron Microscopy (SEM) and Energy Dispersive X-ray (EDX) Spectroscopy Analysis

The surface morphology of the hybrid polyoxometalates (HPOM) was revealed using SEM. In Figure 3(a), the SEM micrograph demonstrated the irregular shape, indicating the presence of sodium tungstate in large aggregates. In Figure 3(b), a heterogeneous morphology was revealed as a rod-like

structure, large fragments and minor presence of granular structure particles. The rod-like structures were reminiscent of the particles of silver acetate [33]. The coarse particle was resembled and identified as sodium tungstate. From Figure 3(b), the aggregated particle and porous area were observed clearly. EDX analysis was employed to determine the elemental composition of HPOM, as shown in Figure 4. In Figure 4, the peaks confirmed the presence of silver (Ag), sodium (Na), tungstate (W) and oxygen (O) in the synthesized HPOM. According to the EDX analysis (Table 1), the synthesized HPOM primarily consists of 20.63% W and 67.72% O. The analysis revealed the presence of transition metal and richness in oxygen content in HPOM. This composition aligned with the presence of transition metal oxyanions that are connected by sharing oxygen atoms and resulted in a polyatomic anion photocatalyst with a high oxygen-rich surface [34].

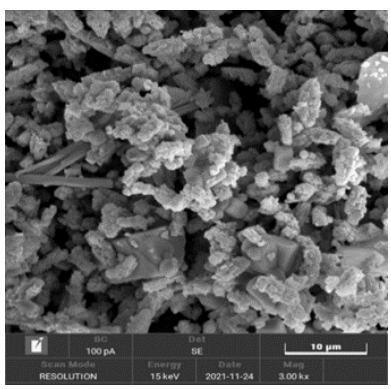

(a)

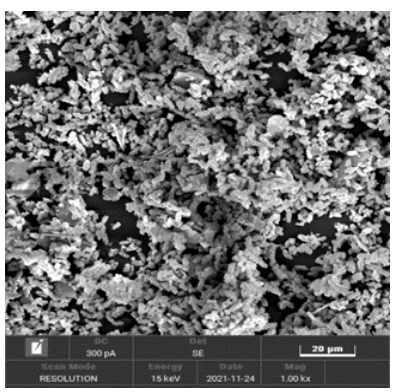

(b)

Figure 3: SEM image of HPOM catalyst of magnification at (a) 1000x and (b) 3000x.

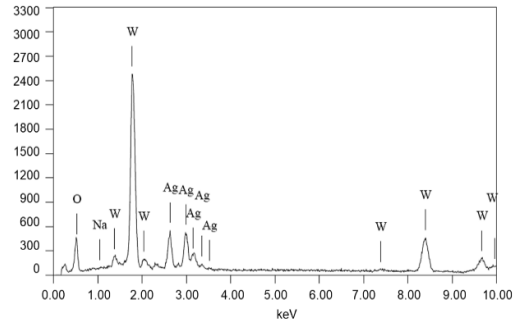

Figure 4: EDX analysis measurement of HPOM.

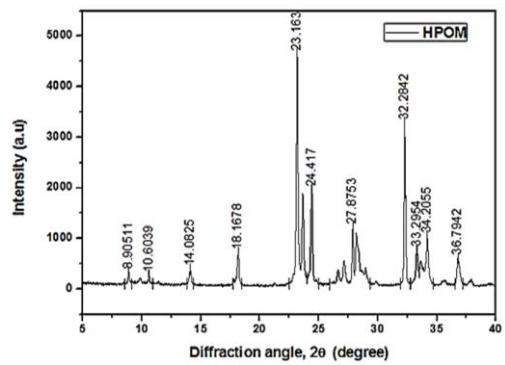

Figure 5: XRD Spectrum of the synthesized HPOM.

Table 1: EDX quantity analysis of the synthesized HPOM.

Element	Atomic (%)	Weight (%)
Silver	11.15	19.75
Sodium	0.50	0.19
Oxygen	67.72	17.79
Tungsten	20.63	62.28

3.1.3 X-Ray Diffraction Analysis (XRD)

The XRD spectrum of HPOM is shown in Figure 5. Within the spectrum, the diffraction peaks were observed at 2θ in the range of 6°–10°, 15°–23°, 25°–30° and 31°–34°, which present the characteristic peak that consistent with Keggin structure [35], [36]. The peak showed at 8.9051° represented the presence of crystalline grains, which are Keggin clusters within the synthesized HPOM [31], while the broad peaks at 15–40° were attributed to small grains, which are also identified as the characteristic peak of Keggin cluster [31], [33]. The XRD analysis was aligned to the crystalline structure of the synthesized HPOM and confirmed with the Keggin structure that exhibited the diffraction peaks such as 8.9051°, 18.1678°, 23.163° and 32.2842° [27], [35], [37].

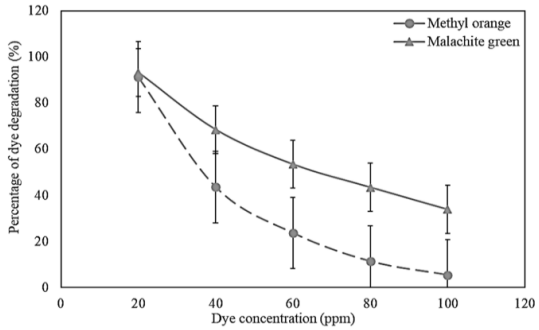

Figure 6: Effect of initial concentration of dye solution on the photocatalytic degradation at 180 min (Experimental condition: HPOM dosage: 0.01 g, reaction temperature: 25 °C).

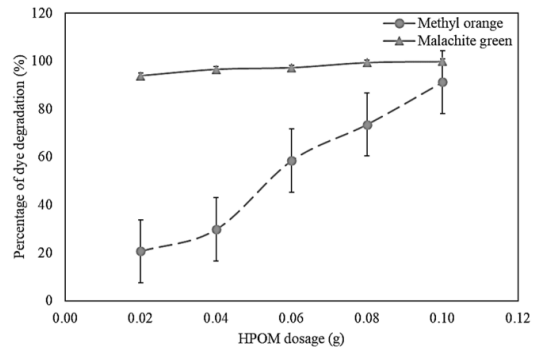

Figure 7: Effect of HPOM dosage on the photocatalytic degradation of MO and MG at 180 min (Experimental condition: Initial dye concentration: 20 ppm, reaction temperature: 25 °C).

3.2 *Effects of Initial Concentration*

The photocatalytic degradation efficiencies of HPOM towards MO and MG at different initial concentrations are outlined in Figure 6. As observed the degradation efficiency of photocatalysts for both dye solutions decreased with increasing the dye concentration. The maximum percentage degradation of MO and MG dye at the highest concentration (100 ppm) were 5.36% and 33.88%, respectively, resulting in the lowest degradation percentages. In contrast, 20 ppm solutions of MO and MG dye exhibited the highest percentage of dye degradation which were 91.25% and 93.19% respectively. Both dye solutions highlighted the same descending trend which was also reported by other relevant literature: the percentage of photocatalytic degradation decreases as the dye concentration increases [22], [38].

The reduction in photodegradation percentage with the increasing dye concentration was associated with the adsorption behavior of dye molecules. Increasing the initial dye concentration resulted in a greater number of dye molecules being adsorbed onto the surface of the photocatalyst [39]. The percentage degradation of dye was influenced by the adsorption of dye and the penetration of UV light onto the surface of the photocatalyst [40]. The dye adsorption onto the catalyst eases the photodegradation process by exciting the dye molecule. However, this process was limited by the availability of active sites on the catalyst thus limiting the absorption of dye molecules [41], [42]. Excessive amounts of dye molecules reduced the UV irradiation penetration, the blocking of the irradiation results in decreased photon availability on the HPOM surface, which in turn diminished the formation of hydroxyl (OH) radicals [43]. HPOM exhibited better photocatalytic degradation toward MG dye compared to MO dye due to its surface-charged properties. HPOM possesses a negatively surface-charged photocatalyst, which promotes the adsorption of cationic dye molecules onto its surface through electrostatic interactions [44].

3.3 *Effects of HPOM Dosage*

The effect of HPOM photocatalyst dosage on MO and MG dye photodegradation was investigated and the absorbance values were examined using a UV-vis spectrophotometer every 10 min interval throughout the experiment. Figure 7 illustrates the percentage of MO and MG degradation over time with different HPOM dosages. The experiment with 100 mg HPOM exhibited the highest percentage of both MO and MG dye degradation which were 91.25% and 99.80%, respectively. The percentage degradation of dyes increased as the HPOM dosage increased. The higher amount of catalyst increased photodegradation activity by providing a greater exposure of active sites due to a larger surface area of the photocatalyst. The enlarge surface area provided facilitated the adsorption of dye molecules on the surface of the photocatalyst, resulting in higher degradation efficiency [26]. Higher exposure of active sites promoted higher absorption of photons from the light and led to a higher production of reactive species like OH radicals and positive holes (h^+), enhancing photodegradation [45]. However, for certain photocatalysts such as TiO_2, the excessive dosage can also lead to

catalyst aggregation, which reduces the availability of active sites on the surface and subsequently hinders photocatalytic degradation [46].

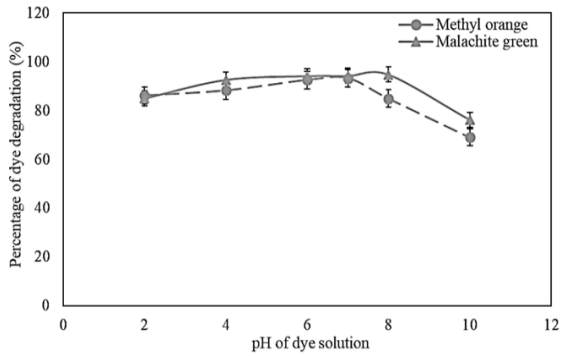

Figure 8: Effect of initial pH of MO and MG dye solution on the photocatalytic activity of dye at 180 min (Experimental condition: Initial dye concentration: 20 ppm, HPOM dosage: 0.010 g, reaction temperature: 25 °C).

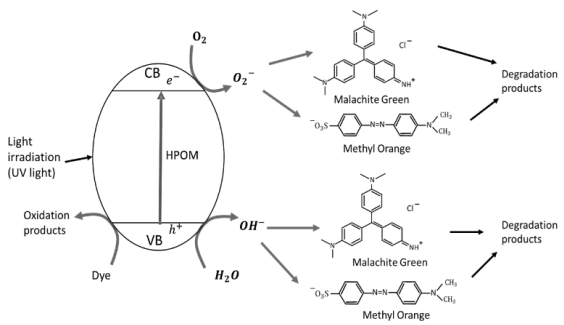

Figure 9: Proposed mechanism of photocatalytic degradation of MO and MG dye by HPOM.

3.4 *Effects of pH*

The effect of pH on the photocatalytic degradation performance of MO and MG dye solution by HPOM is shown in Figure 8. Increasing pH from 2.0 showed the increasing photodegradation of the dye solution for both dyes. In Figure 8, the degradation percentage of MG dye reached the highest when the dye solution was at pH 8, while the degradation percentage of MO recorded the highest at pH 7. The pH of the solution can affect the adsorption of dye molecules onto the surface of the photocatalyst and the oxidation of organic compounds, thus affecting the adsorption of dye molecules onto the surface of the catalyst [47]. The pH can alter the charge on the photocatalyst's surface, thus affecting the adsorption of ions [9]. The hydrogen ions (h^+) in the dye solution at low pH enhanced the surface acidity of HPOM. MO was reported to have an anionic configuration—the degradation rate increases with the increasing of pH value until maximum at optimum pH value. When the pH of the dye solution exceeds pH 7, the MO degradation decreases. Such an observation was mainly attributed to the electrostatic repulsion between the negatively charged MO from the negatively charged photocatalyst under the alkaline condition. The numbers of anionic molecules adsorbed on the surface of the catalyst decreases due to the presence of the hydroxyl group [48]–[51]. Meanwhile, MG possessed a cationic configuration, which its adsorption is favorable in alkaline solution. The positively charged density on the surface of HPOM decreased with increasing pH due to the deprotonation of the catalyst surface and dissociated functional group [52]. When the solution's pH increased, the catalyst's surface was negatively charged. The negatively charged catalyst attracts the cationic dye from the solution. Thus, high degradation of MG was observed in solution with alkaline [48], [53].

3.5 *Proposed mechanism for photocatalytic degradation of MO and MG Dye using HPOM photocatalyst*

According to the experimental results and the previous studies [13], [29], [34], [54], the photocatalytic degradation mechanism of MO and MG dyes was described as a three-step mechanism involving: the adsorption of dye molecules, the adsorption of photons and the generation of electron-hole pairs. The proposed photocatalytic degradation mechanism of dyes was illustrated in Figure 9 and expressed as Equations (1)–(6). Firstly, the MO and MG dye molecules were adsorbed onto the active sites on the surface of the HPOM photocatalyst. The UV light was irradiated onto the HPOM surface, promoting the adsorption of the photons. The continuous photon energy excited the HPOM, facilitating the accessibility of charge transfer as the photon initiated the formation of electrons-hole pairs as follows:

$$HPOM + hv \rightarrow HPOM(h_{VB}^{+} + e_{CB}^{-}) \quad (1)$$

Under the UV light irradiation, high energy photons were absorbed into the HPOM photocatalyst and the electrons from the valence band (VB) were excited to the conduction band (CB) while the photogenerated positive holes remaining in the VB oxidized the dye molecules. This created the reactive intermediates. The recombination of electrons and holes can be avoided by efficient charge separation. When the photogenerated electron-hole pairs were promoted, the photogenerated holes acted as oxidizing agents to oxidize the dye or water molecules attached to the HPOM surface, thus forming the hydroxyl radicals (OH^-). Whilst, the photogenerated electrons converted O_2 into O_2^-, O_2^- attacks and breaks down the dye molecules, contributing to less harmful byproducts [55]. This degradation process contributed to Equations (4)–(6).

$$h^+ + H_2O \rightarrow H^+ + \cdot OH \quad (2)$$

$$e^- + O_2 \rightarrow \cdot O_2^- \quad (3)$$

$$h^+ + \text{Dye} \rightarrow \text{Oxidation product} \quad (4)$$

$$\cdot O_2^- + Dye \rightarrow H_2O + CO_2 + \text{degradation products} \quad (5)$$

$$\cdot OH + Dye \rightarrow H_2O + CO_2 + \text{degradation products} \quad (6)$$

3.6 *Kinetic study*

The kinetics of the photocatalytic process of MO and MG using HPOM were evaluated. The Langmuir-Hinshelwood model was reported in modeling the kinetics of photocatalytic degradation. The initial rate of photocatalytic degradation, r_0, was determined using the Langmuir-Hinshelwood kinetic model and expressed to Equations (7)–(10) as follows [56], [57], [58]. Equation (8) can be expressed by integrating the Equation (7) when the concentration of reactant is low and the denominator of Equation (8) is neglected, which showed the first-order reaction.

$$r_0 = -\frac{dC}{dt} = \frac{k_{cat}K_{LH}C_0}{1+K_{LH}C_0} = k_{app}C_0 \quad (7)$$

$$\ln\left(\frac{C_0}{C}\right) = k_{app}t \quad (8)$$

$$\frac{1}{r_0} = \frac{1}{k_{cat}} + \frac{1}{k_{cat}K_{LH}C_0} \quad (9)$$

$$\frac{1}{k_{app}} = \frac{C_0}{k_{cat}} + \frac{1}{k_{cat}K_{LH}} \quad (10)$$

It was followed by Equations (9) and (10) where k_{app} is the reaction rate, k_{cat} is the rate constant, K_{LH} is the adsorption equilibrium constant, and C_0 is the initial concentration.

In this study, the initial photocatalytic degradation rate was calculated at t =180 minutes. The photocatalytic degradation of both dyes followed with Langmuir-Hinshelwood kinetic model. The equation was rearranged into linear form as Equation (8). As depicted in Figure 10, ln (C_0/C) relationship against time exhibited a linear relationship, followed by the Langmuir-Hinshelwood with the pseudo-first-order kinetic model [26], [56]. In the experiment, a low concentration of reactant was used. For the case of low reactant concentration, Langmuir Hinshelwood with pseudo-first-order was rewritten, and the kinetic plot of ln (C_0/C) against time at a different concentration as in Figure 10 represented the rate constant of reaction equation can be expressed as Equation (8) [59], [60]. Figure 11 demonstrated that the plot of ln (C_0/C) against time was fitted with a straight line, especially in 40 ppm dye solution, resulting in the highest R^2 value. Therefore, the higher value of R^2 indicated a fit to the Langmuir-Hinshelwood model, a well-described photocatalytic degradation of MO and MG by HPOM with a pseudo-first-order kinetic model.

Besides, the plot of $1/k_{app}$ against C_0, as in Figure 12 for different dye concentrations, yielded R^2 values of 0.9327 and 0.9946 for MO and MG, respectively. Such results suggested a linear relationship, thus indicating a well-fitting of the pseudo-first-order reaction to the Langmuir-Hinshelwood mechanism for both dyes. A higher reaction rate was observed in the MG solution than in the MO dye solution because of the surface charge properties of HPOM [26]. The negatively charged surface on HPOM revealed a higher affinity in the adsorption of cationic MG dye molecules through electrostatic interactions, leading to increased photocatalytic degradation [44].

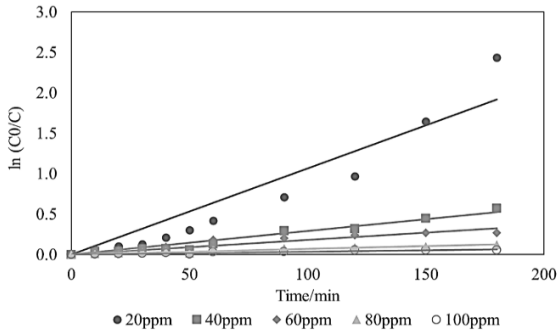

Figure 10: Graph of ln (C_0/C) against a time of photocatalytic degradation of MO (Experimental condition: HPOM dosage: 0.01g, reaction temperature: 25 °C)

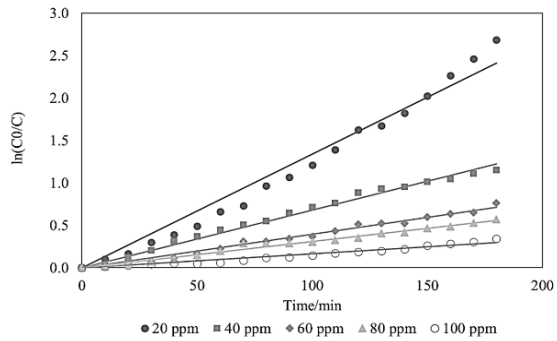

Figure 11: Graph of ln (C_0/C) against a time of photocatalytic degradation of MG (Experimental condition: HPOM dosage: 0.01 g, reaction temperature: 25 °C).

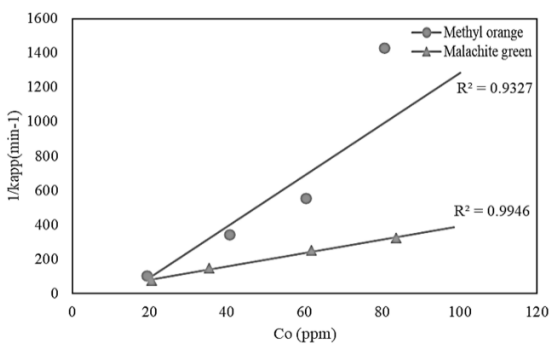

Figure 12: Graph of $1/k_{app}$ against C_0 against a time of photocatalytic degradation of MO and MG.

The values of the rate constant, k_{cat} (min^{-1}), and the coefficient value, $R^{2,}$ were tabulated in Table 2 and Table 3 alongside other works that were reported representing the first-order kinetic model [60], [61]. A comparison between HPOM with different photocatalysts revealed that HPOM had more excellent photocatalytic degradation performance for 20 ppm of MO and MG dye solutions. From Tables 2 and 3, the degradation kinetics of MO and MG dye were present, and R^2 values were larger than 0.9. The accessibility of the catalyst surface for generating electron-hole pairs and hydroxyl radicals was significant in affecting the degradation rate of the dye solution [61]. The higher availability of catalyst surface facilitated in improvement of diffusivity of dye molecules on the surface of the photocatalyst, thereby contributing to a higher degradation rate [45]. By considering the involvement of both anion and cationic dyes, the adsorption and photocatalytic degradation reaction of HPOM were also affected by the electrostatic interactions between dyes and HPOM surface [62]. The synthesized HPOM was negatively charged, thus explained the photodegradation rate of HPOM in MG dye was higher, compared to MO dye.

Table 2: Comparison of various photocatalyst degradation performances of 20 ppm MO dye.

Photocatalyst	Rate Constant, k (min^{-1})	R^2	Ref.
TiO_2	0.00240	0.9790	[63]
PT-13 film	0.00104	0.9993	[64]
HPOM	0.01060	0.9397	This work

Table 3: Comparison of various photocatalytic degradation performances in 20 ppm MG dye.

Photocatalyst	Rate Constant, k (min^{-1})	R^2	Ref.
CuO	0.00808	0.94416	[65]
BiOBr	0.00530	0.96872	[65]
CuCo-500	0.00710	0.9626	[60]
HPOM	0.01340	0.9915	This work

4 Conclusions

The photocatalytic degradation of MO and MG dye was performed using hybrid polyoxometalates (HPOM) as photocatalysts assisted with UV-light irradiation. Through a series of characterizations and experimental analyses, the HPOM photocatalyst was successfully synthesized and the photocatalytic degradation capability of the HPOM photocatalyst was also examined. The structural properties of the HPOM photocatalyst were characterized by FTIR, SEM, and XRD analyses. The functional groups in the photocatalyst sample were identified by FTIR, with the characterization peaks indicating the Keggin structure. For the SEM analysis, silver acetate and sodium tungstate morphologies were confirmed by

revealing rod-like and irregularly aggregated structures, respectively. The EDS analysis also corroborated the elemental composition, identifying the presence of tungstate and oxygen as primary elements by weight composition. XRD analysis demonstrated high crystallinity of HPOM structure, indicating the formation of the Keggin structure in HPOM crystal structure. This work also evaluated the photocatalytic degradation activity of HPOM under different operating conditions assisted by UV light. The increasing initial dye concentration resulted in a decreasing photocatalytic degradation percentage. The highest photodegradation percentage was observed at low concentrations of dye; high concentrations of dye solution had the lowest photodegradation percentage due to a higher amount of dye molecules, causing the blocking of irradiation and reducing the penetration of light. The increased amount of HPOM dosage demonstrated the highest percentage of dye degradation. A larger surface area contributed to a higher availability of active sites on the catalyst surface for the adsorption of dye molecules and photocatalytic degradation. In the effect of initial pH, the photocatalytic degradation of MO and MG dyes revealed the highest percentage at pH 8 and 7, respectively. The increasing pH of the solution contributed to the generation of more hydroxyl groups on the catalyst surface, acting as oxidizing agents in the degradation process. The kinetic study of MO and MG photocatalytic degradation was also investigated, revealing the suitability of the Langmuir Hinshelwood model with pseudo-first-order kinetics. The higher degradation rate of HPOM revealed the higher absorption and oxidation reaction of dye molecules compared to the other photocatalysts. The photocatalytic degradation reaction of HPOM was also affected by the charge of the dye solution. In practical industrial wastewater scenarios, the wastewater contains a mixture of dyes. Through this study, the synthesized HPOM demonstrated high photocatalytic degradation performance, showing a promising ability to remove anionic and cationic dyes which would be one of the attractive applications in industries. While HPOM has potential in wastewater treatment, its reusability and stability should also be focused on minimizing the catalyst waste and promoting a sustainable approach. The findings are crucial for evaluating water treatment technologies. Future research efforts should focus on photocatalytic degradation and developing a modified HPOM photocatalyst in the future to achieve efficient pollutant removal without generating and leaving any chemical residuals in the future.

Acknowledgment

The research was funded by the Ministry of Higher Education, Malaysia (MOHE) Fundamental Research Grant Scheme (FRGS) under grant number FRGS/1/2015/TK02/UNIMAP /02/3 and Universiti Malaysia Perlis (UniMAP).

Author Contributions

All authors contributed to the study conception and design. W.W.L.: methodology, formal analysis, investigation, data curation, writing original draft; S.K.E.A.R.: methodology, writing—reviewing and editing, supervision; Q.H.N.: methodology, supervision; A.D.: investigation; P.Y.H.: Data curation; A.M.N.: writing—review and editing; M.Q.Z.A.S.: Formal Analysis; N.S.A.: writing—review and editing. All authors read and approved the final manuscript.

Conflicts of Interest

The authors declare no conflict of interest.

References

[1] T. Islam, Md. R. Repon, T. Islam, Z. Sarwar, and M. M. Rahman, "Impact of textile dyes on health and ecosystem: A review of structure, causes, and potential solutions," *Environmental Science and Pollution Research*, vol. 30, no. 4, pp. 9207–9242, 2023, doi: 10.1007/s11356-022-24398-3.

[2] L. K. Akula, R. K. Oruganti, D. Bhattacharyya, and K. K. Kurilla, "Treatment of marigold flower processing wastewater using a sequential biological-electrochemical process," *Applied Science and Engineering Progress*, vol. 14, no. 3, pp. 525–542, 2021, doi: 10.14416/j.asep.2021.04.001.

[3] S. S. Affat, "Classifications, advantages, disadvantages, toxicity effects of natural and synthetic dyes: A review," *University of Thi-Qar Journal of Science*, vol. 8, no. 1, pp. 130–135, 2021.

[4] F. Uddin, "Environmental hazard in textile dyeing wastewater from local textile industry," *Cellulose*, vol. 28, no. 17, pp. 10715–10739, 2021, doi: 10.1007/s10570-021-04228-4.

[5] P. O. Oladoye, T. O. Ajiboye, W. C. Wanyonyi, E. O. Omotola, and M. E. Oladipo, "Insights into

remediation technology for malachite green wastewater treatment," *Water Science and Engineering*, vol. 16, no. 3, pp. 261–270, 2023, doi: 10.1016/j.wse.2023.03.002.

[6] K. Maheshwari, M. Agrawal, and A. B. Gupta, *Dye Pollution in Water and Wastewater BT - Novel Materials for Dye-containing Wastewater Treatment*. Singapore: Springer, 2021.

[7] C. Bamroongwongdee, S. Gaewkhem, and P. Siritrakul, "Kinetics, equilibrium, and thermodynamics of methyl orange adsorption onto modified rice husk," *KMUTNB International Journal of Applied Science and Technology*, vol. 11, no. 3, pp. 185–197, 2018, doi: 10.14416/j.ijast.2018.05.002.

[8] L. Wu , X. Liu, G. Lv, R. Zhu, L. Tian, M. Liu, Y. Li, W. Rao, T. Liu, and L. Liao, "Study on the adsorption properties of methyl orange by natural one-dimensional nano-mineral materials with different structures," *Scientific Reports*, vol. 11, no. 1, pp. 1–11, 2021, doi: 10.1038/s41598-021-90235-1.

[9] H. J. Li, J. H. Xu, L. Q. Wang, D. D. Hou, Z. R. Wang, and H. Z. Li, "Adsorption properties of modified ATP-RGO composite aerogel for removal of malachite green and methyl orange from unitary and binary aqueous solutions," *Adsorption Science and Technology*, vol. 2022, 2022, doi: 10.1155/2022/5455330.

[10] S. Yadav and S. Kamsonlian, "Progress on the development of techniques to remove contaminants from wastewater: A review," *Applied Science and Engineering Progress*, vol. 16, no. 3, 2023, Art. no. 6729, doi: 10.14416/j.asep.2023.02.001.

[11] S. Sampurnam, S. Muthamizh, T. Dhanasekaran, D. Latha, A. Padmanaban, P. Selvam, A. Stephen, and V. Narayanan., "Synthesis and characterization of Keggin-type polyoxometalate/zirconia nanocomposites—Comparison of its photocatalytic activity towards various organic pollutants," *Journal of Photochemistry Photobiology A: Chemistry*, vol. 370, pp. 26–40, 2019, doi: 10.1016/j.jphotochem.2018.10.031.

[12] W. S. Koe, J. W. Lee, and W. C. Chong, "An overview of photocatalytic degradation: Photocatalysts, mechanisms, and development of photocatalytic membrane," *Colloid and Interface Science Journal*, vol. 27, pp. 2522–2565, 2019.

[13] Z. Xu, N. Zada, F. Habib, H. Ullah, K. Hussain, N. Ullah, M. Bibi, M. Bibi, H. Ghani, S. Khan, K. Hussain, X. Cai, and H. Ullah, "Enhanced photocatalytic degradation of malachite green dye using silver–manganese oxide nanoparticles," *Molecules*, vol. 28, no. 17, 2023, doi: 10.3390/molecules28176241.

[14] P. L. Hariani, M. Said, Salni, N. Aprianti, and Y. A. L. R. Naibaho, "High efficient photocatalytic degradation of methyl orange dye in an aqueous solution by $CoFe_2O_4$-SiO_2-TiO_2 magnetic catalyst," *Journal of Ecological Engineering*, vol. 23, no. 1, pp. 118–128, 2022, doi: 10.12911/22998993/143908.

[15] A. Hamisu, U. I. Gaya, and A. H. Abdullah, "Bi-template assisted sol-gel synthesis of photocatalytically-active mesoporous anatase TiO_2 nanoparticles," *Applied Science and Engineering Progress*, vol. 14, no. 3, pp. 313–327, 2021, doi: 10.14416/j.asep.2021.04.003.

[16] D. Dodoo-Arhin, T. Asiedu, B. Agyei-Tuffour, E. Nyankson, D. Obada, and J. M. Mwabora, "Photocatalytic degradation of Rhodamine dyes using zinc oxide nanoparticles," *Materials Today Proceedings*, vol. 38, pp. 809–815, 2021, doi: 10.1016/j.matpr.2020.04.597.

[17] P. Niu, D. Wang, A. Wang, Y. Liang, and X. Wang, "Fabrication of bifunctional TiO_2/POM microspheres using a layer-by-layer method and photocatalytic activity for methyl orange degradation," *Journal of Nanomaterials*, vol. 2018, 2018, doi: 10.1155/2018/4212187.

[18] C. Streb, K. Kastner, and J. Tucher, "Polyoxometalates in photocatalysis," *Physical Sciences Reviews*, vol. 4, no. 6, pp. 1–10, 2019, doi: 10.1515/psr-2017-0177.

[19] K. A. Fuad and S. K. E. A. Ab Rahim, "Comparison of HPOM and TiO_2 as Photocatalyst for degradation of methylene blue in aqueous solution," *International Journal of Current Research in Science, Engineering & Technology*, vol. 1, no. Spl-1, p. 300, 2018, doi: 10.30967/ijcrset.1.s1.2018.300-306.

[20] A. V. Anyushin, A. Kondinski, and T. N. Parac-Vogt, "Hybrid polyoxometalates as post-functionalization platforms: From fundamentals to emerging applications," *Chemical Society Reviews*, vol. 49, no. 2, pp. 382–432, 2020, doi: 10.1039/c8cs00854j.

[21] J. Zhang, Y. Huang, G. Li, and Y. Wei, "Recent advances in alkoxylation chemistry of polyoxometalates: From synthetic strategies, structural overviews to functional applications," *Coordination Chemistry Reviews*, vol. 378, pp. 395–414, 2019, doi: 10.1016/j.ccr.2017.10.025.

[22] G. Murmu, S. Samajdar, S. Ghosh, K. Shakeela, and S. Saha, "Tungsten-based Lindqvist and Keggin type polyoxometalates as efficient photocatalysts for degradation of toxic chemical dyes," *Chemosphere*, vol. 346, 2024, Art. no. 140576, doi: 10.1016/j.chemosphere.2023.140576.

[23] N. Hiyoshi, "Fabrication of Keggin-type polyoxometalate membranes at the gas−liquid interface," *Langmuir*, vol. 36, no. 14, pp. 3958–3962, 2020.

[24] J. Arichi, M. M. Pereira, P. M. Esteves, and B. Louis, "Synthesis of Keggin-type polyoxometalate crystals," *Solid State Sciences*, vol. 12, no. 11, pp. 1866–1869, 2010, doi: 10.1016/j.solidstatesciences.2010.01.022.

[25] S. Y. Lai, K. H. Ng, C. K. Cheng, H. Nur, M. Nurhadi, and M. Arumugam, "Photocatalytic remediation of organic waste over Keggin-based polyoxometalate materials: A review," *Chemosphere*, vol. 263, 2021, Art. no. 128244, doi: 10.1016/j.chemosphere.2020.128244.

[26] E. N. A. Azhari, S. K. E. Ab Rahim, A. Duke, and H. P. Yong, "Characterization and kinetic studies on photocatalytic degradation of phenol in aqueous solution," *IOP Conference Series: Materials Science and Engineering*, vol. 932, no. 1, 2020, doi: 10.1088/1757-899X/932/1/012022.

[27] E. I. García-López, G. Marcì, I. Krivtsov, J. Casado Espina, L. F. Liotta, and A. Serrano, "Local structure of supported Keggin and Wells-Dawson heteropolyacids and its influence on the catalytic activity," *Journal of Physical Chemistry C*, vol. 123, no. 32, pp. 19513–19527, 2019, doi: 10.1021/acs.jpcc.9b03659.

[28] D. A. Yaseen and M. Scholz, "Textile dye wastewater characteristics and constituents of synthetic effluents: A critical review," *International Journal of Environmental Science and Technology*, vol. 16, no. 2, 2019, doi: 10.1007/s13762-018-2130-z.

[29] R. Li, Y. Wang, F. Zeng, C. Si, D. Zhang, W. Xu, and J. Shi, "Advances in polyoxometalates as electron mediators for photocatalytic dye degradation," *International Journal of Molecular Sciences*, vol. 24, no. 20, 2023, doi: 10.3390/ijms242015244.

[30] R. Khoshnavazi, L. Bahrami, F. Havasi, and E. Naseri, "H3PW12O40 supported on functionalized polyoxometalate organic-inorganic hybrid nanoparticles as efficient catalysts for three-component Mannich-type reactions in water," *RSC Advances*, vol. 7, no. 19, pp. 11510–11521, 2017, doi: 10.1039/c6ra27519b.

[31] M. Singh, A. Yadav, and C. P. Pradeep, "Keggin cluster modulated photocatalytic activity of aryl sulfonium polyoxometalate hybrids toward dichromate reduction," *Langmuir*, vol. 38, no. 51, pp. 16034–16045, 2022, doi: 10.1021/acs.langmuir.2c02529.

[32] C. Q. Xu, Y. H. Xiao, Y. X. Yu, and W. De Zhang, "The role of hydrogen bonding on enhancement of photocatalytic activity of the acidified graphitic carbon nitride for hydrogen evolution," *Journal of Materials Science*, vol. 53, no. 1, pp. 409–422, 2018, doi: 10.1007/s10853-017-1507-6.

[33] M. Nakano, T. Fujiwara, and N. Koga, "Thermal decomposition of silver acetate: Physico-geometrical kinetic features and formation of silver nanoparticles," *Journal of Physical Chemistry C*, vol. 120, no. 16, pp. 8841–8854, 2016, doi: 10.1021/acs.jpcc.6b02377.

[34] J. Wu, D. Wu, W. Peng, Y. Ji, and H. Tong, "Research progress of polyoxometalates photocatalyst for degradation of organic wastewater," *Applied Chemical Engineering*, vol. 5, no. 1, pp. 92–106, 2022, doi: 10.24294/ace.v5i1.1635.

[35] H. Cai, X. Wu, Q. Wu, and W. Yan, "Synthesis and high proton conductive performance of a quaternary vanadomolybdotungstosilicic heteropoly acid," *Dalton Transactions*, vol. 45, no. 36, pp. 14238–14242, 2016, doi: 10.1039/c6dt02727j.

[36] A. Aouissi, S. S. Al-Deyab, A. Al-Owais, and A. Al-Amro, "Reactivity of heteropolytungstate and heteropolymolybdate metal transition salts in the synthesis of dimethyl carbonate from methanol and CO_2," *International Journal of Molecular Sciences*, vol. 11, no. 7, pp. 2770–2779, 2010, doi: 10.3390/ijms11072770.

[37] D. S. Aher, K. R. Khillare, and S. G. Shankarwar, "Incorporation of Keggin-based H3PW7Mo5O40into bentonite: synthesis, characterization and catalytic applications," *RSC Advances*, vol. 11, no. 19, pp. 11244–11254, 2021, doi: 10.1039/d1ra01179k.

[38] C. Djebbari, E. zouaoui, N. Ammouchi, C. Nakib, D. Zouied, and K. Dob, "Degradation of Malachite green using heterogeneous nanophotocatalysts (NiO/TiO_2, CuO/TiO_2) under solar and microwave irradiation," *SN Applied Sciences*, vol. 3, no. 2, pp. 1–11, 2021, doi: 10.1007/s42452-021-04266-4.

[39] I. Groeneveld, M. Kanelli, F. Ariese, and M. R. van Bommel, "Parameters that affect the photodegradation of dyes and pigments in solution and on substrate – An overview," *Dyes and Pigments*, vol. 210, 2023, Art. no. 110999, doi: 10.1016/j.dyepig.2022.110999.

[40] M. S. Sha, H. Anwar, F. N. Musthafa, H. Al-Lohedan, S. Alfarwati, J. R. Rajabathar, J. Khalid Alahmad, J. J. Cabibihan, M. Karnan, and K. Kumar Sadasivuni, "Photocatalytic degradation of organic dyes using reduced graphene oxide (rGO)," *Scientific Reports*, vol. 14, no. 1, pp. 1–14, 2024, doi: 10.1038/s41598-024-53626-8.

[41] S. R. Sowmya, G. M. Madhu, and M. Hashir, "Studies on nano-engineered TiO_2 photo catalyst for effective degradation of dye," *IOP Conference Series: Materials Science and Engineering*, vol. 310, no. 1, pp. 0–11, 2018, doi: 10.1088/1757-899X/310/1/012026.

[42] R. V. C. Rubi, J. G. Olay, P. B. G. Caleon, R. A. F. De Jesus, M. B. L. Indab, R. C. H. Jacinto, M. S. Sabalones, F. dela Rosa, and N. L. Hamidah, "Photocatalytic degradation of diazinon in g-C3N4/Fe(III)/persulfate system under visible LED light irradiation," *Applied Science and Engineering Progress*, vol. 14, no. 1, pp. 100–107, 2021, doi: 10.14416/J.ASEP.2020.12.008.

[43] A. P. Aziztyana, S. Wardhani, Y. P. Prananto, D. Purwonugroho, and Darjito, "Optimisation of methyl orange photodegradation using TiO_2-zeolite photocatalyst and H_2O_2 in acid condition," *IOP Conference Series: Materials Science and Engineering*, vol. 546, no. 4, 2019, doi: 10.1088/1757-899X/546/4/042047.

[44] M. Taghdiri, "Selective Adsorption and Photocatalytic degradation of dyes using polyoxometalate hybrid supported on magnetic activated carbon nanoparticles under sunlight, visible, and UV irradiation," *International Journal of Photoenergy*, vol. 2017, 2017, doi: 10.1155/2017/8575096.

[45] R. Gusain, N. Kumar, and S. S. Ray, "Factors influencing the photocatalytic activity of photocatalysts in wastewater treatment," *Photocatalysts in Advanced Oxidation Processes for Wastewater Treatment*, pp. 229–270, 2020, doi: 10.1002/9781119631422.ch8.

[46] H. Zhou, H. Wang, C. Yue, L. He, H. Li, H. Zhang, S. Yang, and T. Ma, "Photocatalytic degradation by TiO_2-conjugated/coordination polymer heterojunction: Preparation, mechanisms, and prospects," *Applied Catalysis B*, vol. 344, 2024, Art. no. 123605, doi: 10.1016/j.apcatb.2023.123605.

[47] R. B. Rajput, S. N. Jamble, and R. B. Kale, "A review on TiO_2/SnO_2 heterostructures as a photocatalyst for the degradation of dyes and organic pollutants," *Journal of Environmental Management*, vol. 307, pp. 1–17, 2022, doi: 10.1016/j.jenvman.2022.114533.

[48] A. Mohamed, M. M. Ghobara, M. K. Abdelmaksoud, and G. G. Mohamed, "A novel and highly efficient photocatalytic degradation of malachite green dye via surface modified polyacrylonitrile nanofibers/biogenic silica composite nanofibers," *Separation and Purification Technology*, vol. 210, pp. 935–942, 2019, doi: 10.1016/j.seppur.2018.09.014.

[49] A. Djebli, A. Boudjemaa, H. Bendjeffal, H. Mamine, T. Metidji, H. Bekakria, and Y. Bouhedja, "Photocatalytic degradation of methyl orange using Zn@[Fe(CN)5NO] complex under sunlight irradiation," *Inorganic and Nano-Metal Chemistry*, vol. 50, no. 11, pp. 1115–1122, 2020, doi: 10.1080/24701556.2020.1735428.

[50] P. Muthirulan, C. Nirmala Devi, and M. Meenakshi Sundaram, "Synchronous role of coupled adsorption and photocatalytic degradation on CAC–TiO_2 composite generating excellent mineralization of alizarin cyanine green dye in aqueous solution," *Arabian Journal of Chemistry*, vol. 10, pp. S1477–S1483, 2017, doi: 10.1016/j.arabjc.2013.04.028.

[51] W. A. Khanday, M. J. Ahmed, P. U. Okoye, E. H. Hummadi, and B. H. Hameed, "Single-step pyrolysis of phosphoric acid-activated chitin for efficient adsorption of cephalexin antibiotic," *Bioresource Technology*, vol. 280, pp. 255–259, 2019, doi: 10.1016/j.biortech.2019.02.003.

[52] N. B. Swan and M. A. A. Zaini, "Adsorption of malachite green and congo red dyes from water: Recent progress and future outlook," *Ecological Chemistry and Engineering S*, vol. 26, no. 1, pp. 119–132, 2019, doi: 10.1515/eces-2019-0009.

[53] C. R. Girish, "Multicomponent adsorption and the interaction between the adsorbent and the adsorbate: A review," *International Journal of Mechanical Engineering and Technology*, vol. 9, no. 7, pp. 177–188, 2018.

[54] M. Ghali, C. Brahni, M. Benltifa, F. Dumur, S. Duval, C. Simonnet-Jégat, F. Morlet-Savary, S. Jellali, L. Bousselmi, and J. Lalevée, "New hybrid polyoxometalate/polymer composites for

photodegradation of eosin dye," *Journal of Polymer Science, Part A: Polymer Chemistry*, vol. 57, no. 14, pp. 1538–1549, 2019, doi: 10.1002/pola.29416.

[55] T. O. Ajiboye, O. A. Oyewo, and D. C. Onwudiwe, "Adsorption and photocatalytic removal of Rhodamine B from wastewater using carbon-based materials," *FlatChem*, vol. 29, 2021, Art. no. 100277, doi: 10.1016/j.flatc.2021.100277.

[56] A. P. Aziztyana, S. Wardhani, Y. P. Prananto, D. Purwonugroho, and Darjito, "Optimisation of methyl orange photodegradation using TiO_2-zeolite photocatalyst and H_2O_2 in acid condition," *IOP Conference Series: Materials Science and Engineering*, vol. 546, no. 4, 2019, doi: 10.1088/1757-899X/546/4/042047.

[57] D. F. Ollis, "Kinetics of photocatalyzed reactions: Five lessons learned," *Frontiers in Chemistry*, vol. 6, 2018, doi: 10.3389/fchem.2018.00378.

[58] M. S. F. A. Zamri and N. Sapawe, "Kinetic study on photocatalytic degradation of phenol using green electrosynthesized TiO_2 nanoparticles," *Materials Today Proceedings*, vol. 19, pp. 1261–1266, 2019, doi: 10.1016/j.matpr.2019.11.131.

[59] F. Zhou, C. Yan, T. Liang, Q. Sun, and H. Wang, "Photocatalytic degradation of Orange G using sepiolite-TiO_2 nanocomposites: Optimization of physicochemical parameters and kinetics studies," *Chemical Engineering Science*, vol. 183, pp. 231–239, 2018, doi: 10.1016/j.ces.2018.03.016.

[60] A. Gouasmia, E. Zouaoui, A. A. Mekkaoui, A. Haddad, and D. Bousba, "Highly efficient photocatalytic degradation of malachite green dye over copper oxide and copper cobaltite photocatalysts under solar or microwave irradiation," *Inorganic Chemistry Communications*, vol. 145, 2022, Art. no. 110066, doi: 10.1016/j.inoche.2022.110066.

[61] G. Arroyo-Ortega, J. F. Hernández Paz, I. Olivas Armendariz, H. Camacho-Montes, C. López-Díaz-De León, H. Reyes-Blas, and C. A. Rodríguez-González, "Photocatalytical degradation of methyl orange (MO) using ZnO nanoparticles from alkaline wasted batteries. The effect of the MO, catalyst, and organic loads," *Digest Journal of Nanomaterials and Biostructures*, vol. 17, no. 4, pp. 1241–1248, 2022, doi: 10.15251/DJNB.2022.174.1241.

[62] A. M. Hidalgo, G. León, M. Gómez, M. D. Murcia, E. Gómez, and J. A. Macario, "Removal of different dye solutions: A comparison study using a polyamide nf membrane," *Membranes (Basel)*, vol. 10, no. 12, pp. 1–16, 2020, doi: 10.3390/membranes10120408.

[63] M. Shafique, M. S. Mahr, M. Yaseen, and H. N. Bhatti, "CQD/TiO_2 nanocomposite photocatalyst for efficient visible light-driven purification of wastewater containing methyl orange dye," *Materials Chemistry and Physics*, vol. 278, 2022, Art. no. 125583, doi: 10.1016/j.matchemphys.2021.125583.

[64] Z. A. M. Hir, P. Moradihamedani, A. H. Abdullah, and M. A. Mohamed, "Immobilization of TiO_2 into polyethersulfone matrix as hybrid film photocatalyst for effective degradation of methyl orange dye," *Materials Science in Semiconductor Processing*, vol. 57, pp. 157–165, 2017, doi: 10.1016/j.mssp.2016.10.009.

[65] D. A. Sabit and S. E. Ebrahim, "Fabrication of magnetic BiOBr/$ZnFe_2O_4$/CuO heterojunction for improving the photocatalytic destruction of malachite green dye under LED irradiation: Dual S-scheme mechanism," *Materials Science in Semiconductor Processing*, vol. 163, 2023, Art. no. 107559, doi: 10.1016/j.mssp.2023.107559.